METALS AND MATERIALS International, Vol. 9, No. 3 (2003), pp. 221~226

Cubic to Tetragonal Martensitic Transformation in a Thin Film Elastically Constrained by a Substrate

D. J. Seol[1,*], S. Y. Hu[2], Y. L. Li[2], L. Q. Chen[2], and K. H. Oh[1]

[1] School of Materials Science and Engineering, Seoul National University
San 56-1 Shillim 9-dong, Gwanak-gu, Seoul 151-742, Korea
[2] Department of Materials Science and Engineering, The Pennsylvania State University
University Park, PA 16802, USA

A 3-dimensional phase-field model is developed to describe the cubic to tetragonal martensitic phase transformation in a thin film attached to a substrate. Elasticity solutions are derived for both elastically anisotropic and isotropic thin films with arbitrary domain structures, subject to the mixed boundary conditions for stress-free and constrained states. The model is applied to an Fe-31%Ni alloy system. The nucleation process as well as the final domain structure strongly depends on the substrate constraint. At a smaller undercooling, the increased strain energy effect results in a lower volume fraction of martensite, a finer domain structure and a longer nucleation period.

Keywords: cubic to tetragonal, martensitic transformation, phase-field model, thin film

1. INTRODUCTION

Martensitic transformation (MT) takes place in many engineering materials. The properties of the transformed materials are strongly affected by the martensitic product phase in both bulk and constrained thin film cases [1]. Interest in the martensitic transformation in a thin film elastically constrained by an attached substrate has increased recently due to the growing applications of ferroelectric and ferromagnetic materials, and shape memory alloys.

The martensitic transformation is classified into two groups. One is proper MT and the other improper. The leading transformation mode of the proper MT is a homogeneous stress-free strain which characterizes a change in crystal lattice parameters [2]. The MT in Fe-based alloys is a typical example of proper MT. The crystal lattice rearrangement from *fcc* to *bcc* in Fe-based alloys is fully described by the tetragonal Bain distortion. Khachaturyan *et al*. have developed a theory and simulation model of the proper MT in bulk materials [2]. They investigated with computer simulation the nucleation process, transformation kinetics and final morphologies of MT in a bulk material. But it is known that the phase transformation kinetics and final morphologies change considerably in thin film material due to the confined geometry compared to bulk material [3,4]. The objective of this work is to study how the kinetics and morphologies of the proper MT are affected by the confined geometry of the thin film attached to the substrate. We use a phase-field model to simulate proper MT.

Phase-field models provide a convenient basis for a numerical solution to the complicated pattern evolution of the transforming phases because all the governing equations are solved without interface tracking in the whole space of the system. Phase-field models have been successfully applied to the prediction of martensitic microstructural evolution in bulk materials [1,2,5] and in ferroelectric thin films [6,7]. We develop a 3-dimensional phase-field model to provide a proper description of cubic to tetragonal martensitic transformation in thin film elastically constrained by a substrate. The effects of substrate constraint and undercooling on the final microstructure and transformation kinetics are studied for an Fe-31%Ni alloy.

2. PHASE-FIELD MODEL OF CUBIC-TO-TETRAGONAL MARTENSITIC TRANSFORMATION

In a phase-field approach, the cubic to tetragonal MT is

This article is based on a presentation made in the 2002 Korea-US symposium on the "Phase Transformations of Nano-Materials," organized as a special program of the 2002 Annual Meeting of the Korean Institute of Metals and Materials, held at Yonsei University, Seoul, K orea on October 25-26, 2002.

*Corresponding author: djseol2@snu.ac.kr

represented by the phase fields of three long range order (lro) parameters, η_1, η_2, η_3. The temporal evolution of a phase field, η_i (i = 1,2,3), is described by the time-dependent Ginzburg-Landau kinetic equation [8]:

$$\frac{\partial \eta_i(\vec{r},t)}{\partial t} = -L_i\frac{\delta F}{\delta \eta_i(\vec{r},t)} + \xi_i(\vec{r},t)$$
$$= -L_i\left(\frac{\partial f}{\partial \eta_i} - \beta_i\nabla^2\eta_i + \mu_{el}\right) + \xi_i(\vec{r},t) \quad (1)$$

where $\vec{r}$ is a position vector, F is the total specific free energy of a the system, L_i the phase-field mobility, $\xi_i(\vec{r}, t)$ the thermal noise term, β_i the gradient energy coefficient, and μ_{el} is a derivative of the elastic energy density function with respect to the lro parameters. The total free energy of a system consists of the bulk chemical free energy, interfacial energy, elastic energy, and the free energy associated with an applied field, etc. The interfacial energy is related to $\beta_i\nabla^2\eta_i$. The chemical free energy density, f, is approximated by a Landau-type fourth-order polynomial consisting of the cubic symmetry invariants of the lro parameters [2],

$$f(\eta_1,\eta_2,\eta_3)^* = f(0,0,0)^* + \frac{1}{2}A_1^*(\eta_1^2+\eta_2^2+\eta_3^2)$$
$$-\frac{1}{3}A_2^*(\eta_1^3+\eta_2^3+\eta_3^3) + \frac{1}{4}A_3^*(\eta_1^2+\eta_2^2+\eta_3^2)^2 \quad (2)$$

where $f(\eta_1, \eta_2, \eta_3)^*=f(\eta_1, \eta_2, \eta_3)/|\Delta f|$, $|\Delta f|$ is the transformation driving force defined as $|\Delta f| = /f(\eta_0, 0, 0) - f(0, 0, 0)|$, which is the difference between the free energy minimum and the free energy of the parent phase, η_0 is the equilibrium value of the lro parameter in the martensite phase, and A_1^*, A_2^* and A_3^* are the dimensionless parameters. Eq. 2 provides a local minimum at $\eta_1=\eta_2=\eta_3=0$ corresponding to the metastable parent phase and global minima at $\eta_1=\eta_0$, $\eta_2=\eta_3=0$, $\eta_2=\eta_0$, $\eta_1=\eta_3=0$, $\eta_3=\eta_0$, $\eta_1=\eta_2=0$ corresponding to the three orientation variants of the stable martensitic phase. To describe the elastic energy caused by the local evolution of microstructure, the stress-free strain needs to be defined. The stress-free strain caused by the change of crystal lattice parameter due to the cubic to tetragonal lattice rearrangement is characterized by,

$$\varepsilon_{ij}^0(\vec{r}) = \sum\varepsilon_{ij}^{\eta}(p)\left(\frac{\eta_p}{\eta_0}\right) = \frac{\eta_1(\vec{r})}{\eta_0}\begin{bmatrix}\varepsilon_3 & 0 & 0\\ 0 & \varepsilon_1 & 0\\ 0 & 0 & \varepsilon_1\end{bmatrix} + \frac{\eta_2(\vec{r})}{\eta_0}\begin{bmatrix}\varepsilon_1 & 0 & 0\\ 0 & \varepsilon_3 & 0\\ 0 & 0 & \varepsilon_1\end{bmatrix}$$
$$+\frac{\eta_3(\vec{r})}{\eta_0}\begin{bmatrix}\varepsilon_1 & 0 & 0\\ 0 & \varepsilon_1 & 0\\ 0 & 0 & \varepsilon_3\end{bmatrix} \quad (3)$$

where, $\varepsilon_1=(a-a_c)/a_c$, $\varepsilon_3=(c-a_c)/a_c$, a and c are the crystal lattice parameters of the tetragonal stress-free martensitic phase, and a_c is the crystal lattice parameter of the cubic parent phase.

In linear elasticity, the stress σ_{ij} is related to the elastic strain by Hookes law:

$$\sigma_{ij} = c_{ijkl}(\varepsilon_{kl}(\vec{r}) - \varepsilon_{kl}^0(\vec{r})) \quad (4)$$

where $\varepsilon_{kl}(\vec{r})$ is the total strain measured with respect to the undistorted reference lattice of the parent phase. If we assume conceptually that the total strain is zero at every position, the film does not have any elastic deformation before and after the phase transformation, while the transformed area with non-zero stress-free strain suffers stress field. The total strain can be separated into homogeneous and heterogeneous strains [9]:

$$\varepsilon_{ij}(\vec{r}) = \bar{\varepsilon}_{ij} + \delta\varepsilon_{ij}(\vec{r}) \quad (5)$$

where the heterogeneous strain, $\delta\varepsilon_{ij}(\vec{r})$, is defined so that

$$\int_V \delta\varepsilon_{ij}(\vec{r})d^3r = 0 \quad (6)$$

where V is the total volume of the system concerned. The homogeneous strain is the uniform macroscopic strain characterizing the macroscopic shape and volume change associated with the total strain. If the thin film is coherent with the substrate, the macroscopic shape deformation of the film in the film plane, $\bar{\varepsilon}_{ij}$, is totally controlled by the sufficiently thick substrate. For example, for a cubic substrate of lattice parameter a_s, and a thin film with a stress-free lattice parameter a_f, $\bar{\varepsilon}_{ij}$ is given by $\bar{\varepsilon}_{11}=\bar{\varepsilon}_{22}=(a_s-a_f)/a_s$, $\bar{\varepsilon}_{12}=0$. The macroscopic shape deformation of the film along x_3 direction is determined by both the substrate constraint and the domain structure in the film. Here we choose the quantity of $\bar{\varepsilon}_{i3}$ in such a way that it makes $c_{i3kl}\bar{\varepsilon}_{kl}=0$. The strain and displacement relationship gives the following equation:

$$\delta\varepsilon_{ij}(\vec{r}) = \frac{1}{2}\left[\frac{\partial u_i(\vec{r})}{\partial r_j} + \frac{\partial u_j(\vec{r})}{\partial r_i}\right] \quad (7)$$

where $u_i(\vec{r})$ denotes the ith component of displacement.

The mechanical equilibrium equations with respect to the elastic displacements are expressed as

$$\frac{\partial \sigma_{ij}}{\partial r_j} = 0 \quad \text{where } i=1,2,3 \quad (8)$$

where r_j is the jth component of $\vec{r}$. The stress-free boundary condition at the top surface of the film is given by

$$\sigma_{i3}\big|_{x_3=h_f} = 0 \quad \text{where } i=1,2,3 \quad (9)$$

where h_f is the film thickness along the film surface normal (x_3) direction (see Fig. 1). Since the elastic perturbation resulting from the heterogeneous strain disappears in the substrate far from the film-substrate interface, the fol-

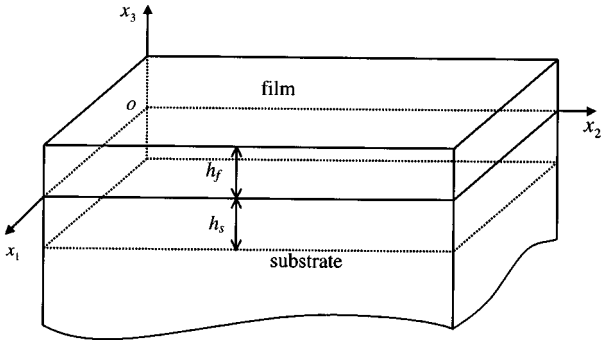

Fig. 1. Schematic illustration of thin film coherently constrained by substrate.

lowing condition is used to describe the constraint of the substrate

$$u_i\big|_{x_3=-h_s} = 0 \quad \text{where } i=1,2,3 \tag{10}$$

where h_s is the distance from the film-substrate interface into the substrate, beyond which the elastic deformation is ignored (see Fig. 1).

To solve Eqs. 8-10, two elastic solutions are superposed [6]. One solution is from Khachaturyans microelasticity theory [9] within $0 < x_3 < h_f$ and another is from the elastic solution for an infinite plate of thickness h_f+h_s, satisfying the two boundary conditions. Consequently, the elastic energy in the constrained thin film can be calculated from Eqs. 4, 5, and 7.

3. SIMULATION PROCEDURES

The dimensionless form of Eq. 1 becomes

$$\frac{\partial \eta_i(\vec{r}^*,t^*)}{\partial t^*} = -\left(\frac{\partial f^*}{\partial \eta_i} - \beta_i^* \nabla^{*2}\eta_i + \mu_{el}^*\right) + \xi_i^*(\vec{r}^*,t^*) \tag{11}$$

where $r^* = r / l_0$, $t^*=tL\,|\Delta f|$ and $\beta_i^* = \beta_i / ((\Delta x)^2|\Delta f|)$, where l_0 is the grid spacing.

Taking a Foutier-transform of both sides of Eq. 11 gives

$$\frac{\partial \eta_i(\vec{g}^*,t^*)}{\partial t^*} = -\left(\left(\frac{\partial f^*}{\partial \eta_i}\right)_{\vec{g}^*} + \beta_i^*(g^*)^2\eta_i(\vec{g}^*,t^*) + \mu_{el}^*(\vec{g}^*)\right) + \xi_i^*(\vec{g}^*,t^*) \tag{12}$$

where g^* is the magnitude of $\vec{g}^*$, $\eta_i(\vec{g}^*,t^*)$, $\mu_{el}^*(\vec{g}^*)$ $\xi_i^*(\vec{g}^*,t^*)$ are the Fourier transforms of $\eta_i(\vec{r}^*,t^*)$, $\mu_{el}^*(\vec{r}^*)$ and $\xi_i^*(\vec{r}^*,t^*)$, respectively. The above equation can be efficiently solved using a semi-implicit method [10],

$$\eta_i(\vec{g}^*,t^*+\Delta t^*) = \frac{\eta_i(\vec{g}^*,t^*) - \Delta t^*\left[\left(\frac{\partial f^*}{\partial \eta_i}\right)_{\vec{g}^*} + \mu_{el}^*(\vec{g}^*)\right]}{1+\beta_i(g^*)^2\Delta t^*} + \tilde{\xi}_i^*(\vec{g}^*,t^*) \tag{13}$$

where $\tilde{\xi}_i^*(\vec{g}^*,t^*) = \Delta t^*\xi_i^*(\vec{g}^*,t^*)/(1+\beta_i(g^*)^2\Delta t^*)$ and Δt^* is the time step for integration.

In the computer simulations, 128×128×32 discrete grid points are used, and periodic boundary conditions are applied along the x_1 and x_2 axes. The dimensionless grid spacing in real space is chosen as $\Delta x_1/l_0 = \Delta x_2/l_0 = 1.0$ and $\Delta x_3/l_0 = 0.5$ and Δt^* is chosen as 0.01. The transformation strains used in this study are those of Fe-31%Ni alloy with ε_1=0.1322 and ε_3= –0.1994 [11]. The elastic constants of the Fe-31%Ni alloy are reported as $c_{11}=1.404\times10^{11}$ Pa and $c_{12}=0.84\times10^{11}$ Pa [12]. The dimensionless parameters A_1^*, A_2^* and A_3^* in the chemical free energy equation are chosen as 0.1, 1.65 and 0.8, respectively, so that η_0=2 and $|\Delta f^*| = |f^*(\eta_0, 0, 0) - f^*(0, 0, 0)|$=1.0, where $|\Delta f^*|$ is the dimensionless form of the transformation driving force. The free energy function has local minimum for the parent phase and global minima for the martensitic phase. The gradient energy coefficient β_i^* is chosen as 0.5 from the diffuse interface description of the Fe-31%Ni alloy [2]. Gaussian random noise is applied for the time period of $t^* = 2.0$ to simulate the nucleation of the martensitic phase. To investigate the effect of undercooling on the martensitic microstructural evolution, a dimensionless ratio between the elastic energy and chemical energy, ζ, is introduced [2].

$$\zeta = \frac{c_{ijkl}\varepsilon_{ij}^0\varepsilon_{kl}^0}{\Delta f} \tag{14}$$

The degree of substrate constraint is measured by the average lattice mismatch between the film and the substrate, $\bar{\varepsilon}_{ij}$, for a given h_s. For simplicity, we considered the case of $\bar{\varepsilon}_{11}=\bar{\varepsilon}_{22}=\bar{\varepsilon}$ and $\bar{\varepsilon}_{12}$=0. Under such a constraint, there are three tetragonal variants, which are labeled η_1, η_2 and η_3, with their tetragonal axes parallel to x_1[100], x_2[010] and x_3[001], respectively.

4. RESULTS AND DISCUSSION

The effect of substrate constraint on microstructure has been investigated with the Fe-31%Ni material when ζ=10. Fig. 2 shows the change in microstructure with respect to different mismatch strains between film and substrate at t^*=15. The microstructure and volume fraction of each domain are strongly dependent on the mismatch strain. When the mismatch strain is zero, the martensitic phase consists of 50 % η_1 and 50 % η_2 domains. The two domains in Fig. 2(a) are alternating {110} twin-related orientation variants and form polytwinned plates. As the mismatch strain becomes more tensile, η_3 domain becomes more favorable and the volume fraction of the η_3 domain increases up to 31 % and 75 % of the total martensitic phase as shown in Figs. 2(b) and (c), respectively.

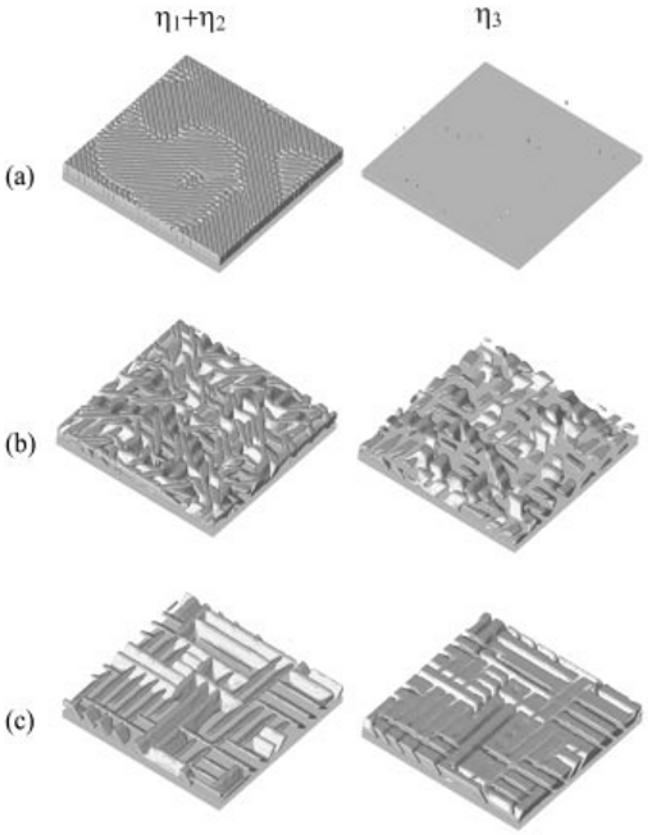

Fig. 2. Microstructures obtained at various substrate constraints with transformation strain of the Fe-31%Ni material when $\zeta = 10$ and $t^* = 15$: (a) $\bar{\varepsilon} = 0.0$; (b) $\bar{\varepsilon} = 0.02$; and (c) $\bar{\varepsilon} = 0.05$.

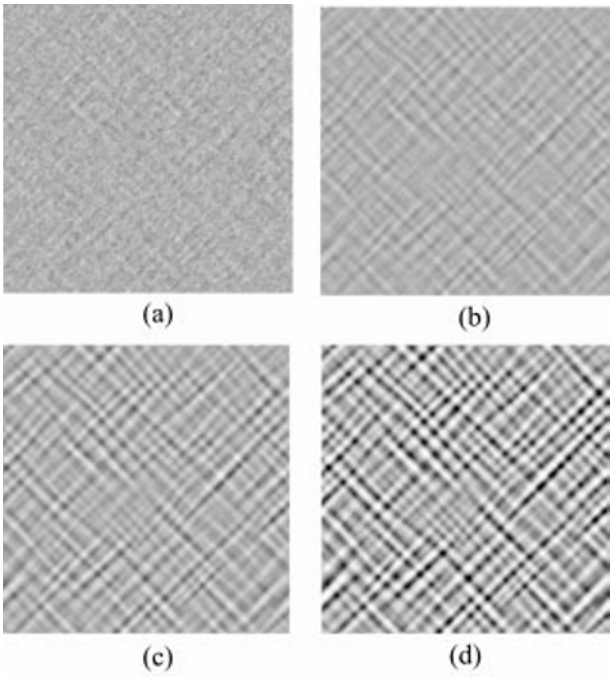

Fig. 3. Initial microstructure evolution of martensitic transformation on top surface without mismatch strain: (a) t^*=1.0; (b) t^*=2.0; (c) t^*=2.5; and (d) t^*=3.0.

Table 1. Change in domain volume fraction in Fig. 3

	(a) t^*=1.0	(b) t^*=2.0	(c) t^*=2.5	(d) t^*=3.0
Parent phase	99.99 %	95.6 %	91.7 %	53.4 %
η_1 domain	0.008 %	2.2 %	4.1 %	23.4 %
η_2 domain	0.008 %	2.2 %	4.2 %	23.2 %

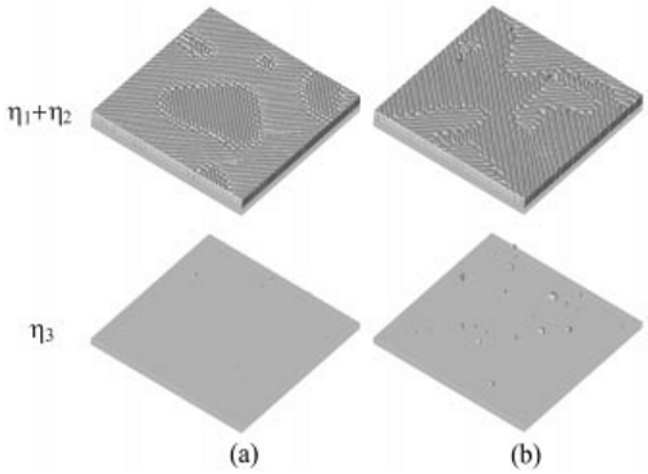

Fig. 4. Domain structures at different undercoolings of (a) ζ=15 and (b) ζ=5 with mismatch strain of 0.0 when t^*=15.

Fig. 3 shows the initial microstructural evolution of the martensitic transformation on the top surface without mismatch strain. The dark and bright fields correspond to the η_1 and η_2 domains, respectively, transformed from the initial parent phase the gray area. At each calculation time, the volume fraction of each domain is listed in Table 1. From the very early stage of nucleation, the η_1 and η_2 domains coexist, suggesting the presence of two variants. A single variant nucleus would create a long-range stress field with large strain energy proportional to the nucleus volume [2]. Therefore complex nuclei are more favorable in terms of their accommodation of transformation strain. The η_1 nuclei are always accompanied by η_2 nuclei in the vicinity or vice versa, called complex nuclei, as shown in the figure.

Fig. 4 shows the domain structures at the different undercoolings of ζ=15 and ζ=5 with the mismatch strain of 0.0 when t^*=15. The η_1 and η_2 domains make zigzag-shaped polytwinned plates [2]. When the undercooling is small (ζ=15), the sizes of the η_1 and η_2 domains are smaller than those in the system under larger undercooling (ζ=5), because of the increase in the relative role of the transformation strain energy. In the system under larger undercooling, the volume fraction of the η_3 domain is higher than that in the system under smaller undercooling, because larger undercooling leads to an increase in the fraction of all domains, which will be clearly shown in Figs. 6 and 7.

Fig. 5 shows the domain structures at different undercoolings of ζ=15 and ζ=5 with the mismatch strain of 0.04 when

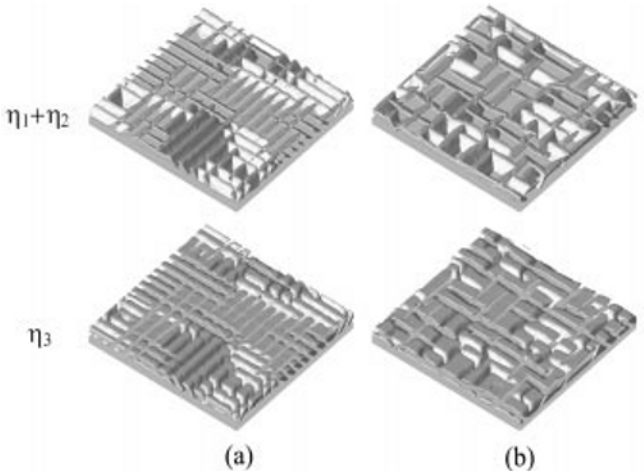

Fig. 5. Domain structures at different undercoolings of (a) ζ=15 and (b) ζ=5 with mismatch strain of 0.04 when t^*=15.

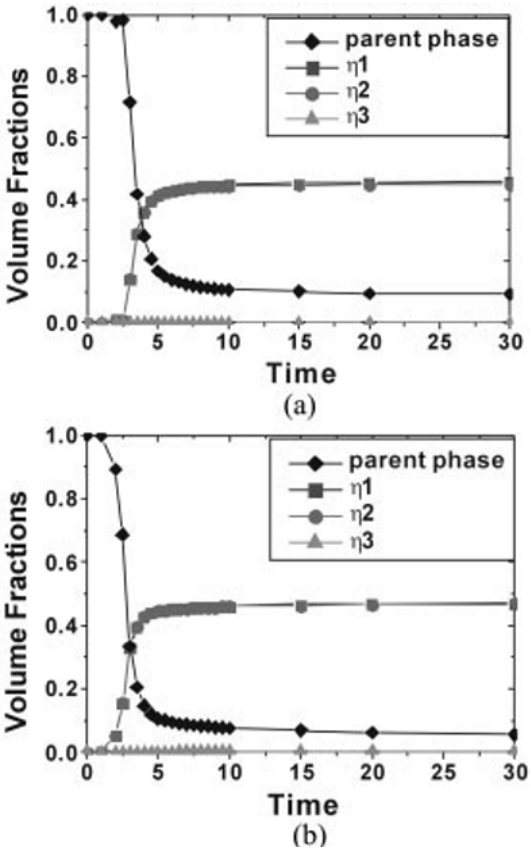

Fig. 6. Change in domain volume fractions versus time without mismatch strain: (a) ζ=15 and (b) ζ=5.

t^*=15. As the mismatch strain increases compared to the case in Fig. 4, many rectangular η_3 domains are observed on the top surface. The transformation strain energy the η_3 domains is accommodated by these adjacent η_1 and η_2 domains. But these three domains do not nucleate at the same time as do the complex nuclei. The large tensile lattice mismatch makes the η_3 domains nucleate first as is shown

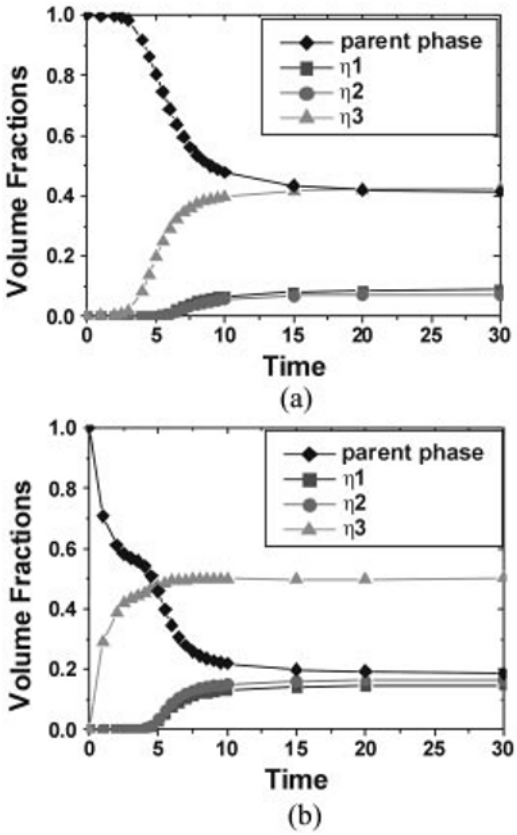

Fig. 7. Change in domain volume fractions versus time with $\bar{\varepsilon}$ = 0.04: (a) ζ=15 and (b) ζ=5.

clearly in Fig. 7. Obviously, we can also see that the domain size is finer under smaller undercooling (ζ=15) compared to that under larger undercooling (ζ=5) at the mismatch strain of 0.04 as it was without mismatch strain.

Figs. 6 and 7 show the change in domain volume fractions versus time when $\bar{\varepsilon}$=0.0 and $\bar{\varepsilon}$=0.04, respectively. The kinetic curves with zero mismatch strain show the simultaneous development of the η_1 and η_2 domains after an incubation period (Fig. 6). When $\bar{\varepsilon}$=0.04, the kinetic curves show that the η_1 and η_2 domains develop after the η_3 domain forms first (Fig. 7). Because of the large tensile lattice mismatch, the η_3 domains nucleate first as single variant nuclei. In both cases, once the transformation starts after the nucleation, the transformation is completed in a short period of time. The incubation period becomes longer as ζ increases, because the increased ζ means increased elastic energy compared to chemical energy. The small undercooling (ζ=15) results in less volume fraction in the martensitic phase, and finer microstructures due to the increased elastic energy effect.

5. CONCLUSION

A 3-D phase-field model for the cubic to tetragonal martensitic transformation is developed to predict the evolution

of martensitic morphology in thin film elastically constrained by a substrate. The microstructure strongly depends on the substrate constraint represented by the mismatch strain. With the transformation strain of the Fe-31%Ni alloy, the martensitic phase in the film consists of polytwinned plates formed by alternating {110} twin-related η_1 and η_2 variants under zero mismatch strain, and the fraction of η_3 increases as the mismatch strain becomes tensile. Strain accommodation starts from the nucleation stage by forming complex nuclei of η_1 and η_2 under zero mismatch strain. When the lattice mismatch is 0.04, single variant η_3 domains nucleate first as single variant nuclei. As the transformation continues, the transformation strain energy of the η_3 domains is more accommodated by these subsequently forming η_1 and η_2 domains beside the η_3 domains. The increase in ζ, which means the undercooling becomes smaller, results in less martensitic volume fraction, finer domain morphology and a longer incubation period due to the increased strain energy effect.

ACKNOWLEDGMENT

The authors are grateful for the financial support of the National Research Laboratory Project and the POSCO Steels Research Fund through the Research Institute of Advanced Materials at Seoul National University, and of the US National Science Foundation under grant number DMR-01-22638.

REFERENCES

1. A. Artemev, Y. Wang, and A. G. Khachaturyan, *Acta mater.* **48**, 2503 (2000).
2. A. Artemev, Y. Jin, and A.G. Khachaturyan, *Acta mater.* **49**, 1165 (2001).
3. K. Binder, *J. Non-Equilib. Thermodyn*. **23**, 1 (1998).
4. D. J. Seol, S. Y. Hu, Y. L. Li, J. Shen, K. H. Oh, and L. Q. Chen, *Metals and Materials Int.* **9**, 61 (2003).
5. Y. M. Jin, A. Artemev, and A.G. Khachaturyan, *Acta mater.* **49**, 2309 (2001).
6. Y. L. Li, S. Y. Hu, Z. K. Liu, and L. Q. Chen, *Acta mater.* **50**, 395 (2002).
7. Y. L. Li, S. Y. Hu, Z. K. Liu, and L. Q. Chen, *Appl. Phys. Lett*. **78**, 3878 (2001).
8. L. Q. Chen, *Annu. Rev. Mater. Res*. **32**, 113 (2002).
9. A.G. Khachaturyan, *Theory of Structural Transformations in Solids*, p. 198, John Wiley & Sons, New York, USA (1983).
10. L. Q. Chen and J. Shen, *Comput. Phys. Commun*. **108**, 147 (1998).
11. J. E. Breedis and C. M. Wayman, *Trans. Metall. Soc. AIME* **224**, 1128 (1962).
12. G. Hausch and H. Warlimont, *Acta metall*. **21**, 401 (1973).